JOURNAL OF AIRCRAFT
Vol. 43, No. 6, November–December 2006

Synthetic Jet Control Effectiveness on Stationary and Pitching Airfoils

A. Rehman* and K. Kontis†
University of Manchester, Manchester, M60 1QD England, United Kingdom

DOI: 10.2514/1.20333

A computational study has been conducted to investigate the control effectiveness of a synthetic jet on a stationary and a pitching NACA 0015 airfoil at a Reynolds number of 360,000 based on the chord length. For the stationary airfoil, the optimum location of the synthetic jet was at 28% of the chord length. The nondimensional maximum forcing amplitude was 0.75 and the nondimensional forcing frequency was 18.67. The increase in lift was more pronounced at higher incidences, whereas the effectiveness of the synthetic jet reduced at lower incidences. Imparting movement of flow far away from separation point was useful for lift enhancement. The location of the jet close to separation point was suitable for drag reduction. The pitching airfoil was driven in a periodic cycle corresponding to $\alpha = 5 + 10\sin(0.15t)$. A synthetic jet with nondimensional maximum forcing amplitudes of 0.75 and 1.88, and nondimensional forcing frequencies of 18.67 and 31.13 was employed. The higher frequency was suitable for lift enhancement whereas the higher amplitude was suitable for drag reduction. A single synthetic jet was not able to suppress the vortex formation and shedding; however, the overall airfoil performance was enhanced. The k–ω shear-stress transport model successfully predicted the flow events of both airfoil configurations.

Nomenclature

A_o	=	nondimensional synthetic jet maximum forcing amplitude, V_{jo}/U_∞
C_D	=	drag coefficient, $D/q_\infty S$
C_L	=	lift coefficient, $L/q_\infty S$
C_M	=	moment coefficient, $M/q_\infty Sc$
C_p	=	pressure coefficient
c	=	chord, m
f	=	frequency, Hz
k	=	turbulent kinetic energy, m^2/s^2
L_j	=	nondimensional synthetic jet location, $(x/c) \times 100$
Re	=	Reynolds number, $\rho U_\infty c/\mu$
t	=	time, s
U_∞	=	freestream velocity, m/s
V_{jo}	=	synthetic jet maximum forcing velocity of the blowing-suction cycle, m/s
x	=	axial distance along the airfoil chord from leading edge, m
Y^+	=	distance of first node from body surface
α	=	angle of attack, deg
ε	=	dissipation rate of the turbulent kinetic energy, m^2/s^3
κ	=	reduced pitching oscillation frequency, $fc/2U_\infty$
μ	=	kinetic viscosity of the fluid, $\text{kg/m} \cdot \text{s}$
ρ	=	density, kg/m^3
ω	=	specific dissipation rate, 1/s
ω_j	=	nondimensional synthetic jet forcing frequency, fc/U_∞

Introduction

In an airfoil, the maximum achievable lift is ultimately limited by the ability of the flow to follow the curvature of the airfoil. When it cannot, the flow would separate [1,2]. Flow separation over an aircraft wing usually causes a significant loss of lift and increase in drag, which limits the aerodynamic performance of the aerospace vehicle (takeoff and landing distances, maximum and sustained turn rates, climb and glide rates, flight ceiling, etc.). Delaying or eliminating separation entirely would increase lift and reduce drag, hence increasing the aerodynamic performance of lifting surfaces [3]. Dynamic stall occurs when the airfoil is pitched above its natural static stall angle [4–6]. Accurate prediction and, possibly, control of dynamic stall could enhance the performance of lifting surfaces in various engineering applications [7,8]. For example, the maneuverability of fighter aircraft could be enhanced if the unsteady air loads generated by dynamic stall are used in a controlled manner. Effective stall control of the retreating blade of a helicopter rotor could also increase the maximum flight speed by reducing rotor vibrations and power requirements [9]. In the past, various attempts have been made to manipulate the flow over stationary as well as pitching airfoil using various types of passive techniques such as vortex generators [10], sharp leading edge airfoils [11], slatted airfoils [12], dynamic deformed leading edge and slotted airfoils , and variable droop leading edge with Gurney flap [14], and active flow control devices such as pulsed microjets [15], pulsed vortex generator jets [16], plasma actuators [17], and unsteady suction and blowing [18].

In the present paper, the authors examined the effectiveness of a single synthetic jet for separation control on both stationary and pitching NACA 0015 airfoils. The synthetic jet has the following distinct advantages over other passive and active control devices: 1) zero net mass flux, which eliminates the need for plumbing and therefore it offers the potential for weight saving; 2) nonzero mean momentum flux; 3) increased actuator robustness; and 4) extremely low actuation power requirements [19].

Computational Approach

Flow was assumed to be incompressible, viscous, two-dimensional, steady for the stationary airfoil without synthetic jet, and unsteady for the stationary airfoil with synthetic jet and the pitching airfoil with and without synthetic jet. There is no external source that transfers heat into the system; therefore the energy equation was not considered. Fluent provides two options for solvers: a segregated and a coupled solver. For the flow conditions being investigated, the segregated solver was selected. The implicit method was used. By using this method, all the fluxes and source terms were evaluated in terms of the unknown variable values at the new time level. The pressure and velocity were coupled using the

Received 1 October 2005; revision received 8 December 2005; accepted for publication 8 December 2005.

*Ph.D. Student, School of Mechanical, Aerospace and Civil Engineering.
†Associate Professor and Research Group Head, Experimental Aerodynamics and Advanced Measurement Technology Laboratory. Member AIAA.

Simple algorithm. This algorithm uses a guess-and-correct procedure for the calculation of pressure on the staggered grid arrangement. For the discretization of the model equations, Quick scheme was used instead of the first-order or second-order upwind scheme [20,21]. This scheme is of higher order of accuracy and can minimize false diffusion errors but it is less computationally stable. In contrast, the upwind scheme is always bounded with the major drawback of giving erroneous results when the flow is not aligned with the grid lines. Therefore, it is probably not suitable for the present investigation due to the high vorticity of the flow field. Finally, the time step was set to 0.0001 s for all unsteady simulations performed in the present study to ensure that a full cycle of the actuator was completely calculated.

Model Geometry and Flow Domain

Gambit was used to create the geometric models for both airfoil configurations. The stationary airfoil was placed at the center of the computational domain. Each lateral boundary was located at $15c$ from the center of the domain. The inflow and outflow boundaries were located $10c$ upstream and $20c$ downstream of the airfoil, respectively. For the stationary NACA 0015 configuration, mesh convergence was achieved with 160 nodes on each surface of the airfoil. A grid spacing adjacent to the airfoil surface corresponded to $Y^+ = 1$ was achieved. For the pitching NACA 0015 configuration, 110 nodes were placed on each surface of the airfoil. The first row of grid points, adjacent to the airfoil surface, had a minimum height of $0.0001c$ to ensure Y^+ equal to 25. For "Face 2" (outer portion of the circle), a comparative coarse grid was used. Detailed views of the final mesh for the stationary and pitching airfoils are presented in Fig. 1.

Turbulence Model Selection Studies

The lift and drag coefficients were computed at angles of attack ranging from 0 to 4 deg using all available turbulence models within Fluent [22]. The computed results along with experimental data [23] are compared in Fig. 2. All models successfully predicted C_L at all incidences; however, only the standard k–ω, k–ω shear-stress transport (SST), and k–ε realizable models produced results that were relatively close to the experimentally measured drag coefficients. Because the k–ω SST is a modified version of the k–ω standard model, and k–ε realizable is an improved version of the k–ε standard and renormalization group (RNG) k–ε models, the authors decided to use both k–ω SST and k–ε realizable to compute the flow parameters.

Boundary Conditions

The velocity inlet boundary condition was used for all numerical simulations. The velocity inlet boundary condition is intended for use with incompressible flows where the magnitude and direction of the inlet velocity is known. This boundary condition allows the stagnation, or total properties of the flow to rise to whatever value is necessary to generate the prescribed velocity distribution. At the exit, the outflow boundary condition was employed. This boundary condition could be used to model situations where the details of the

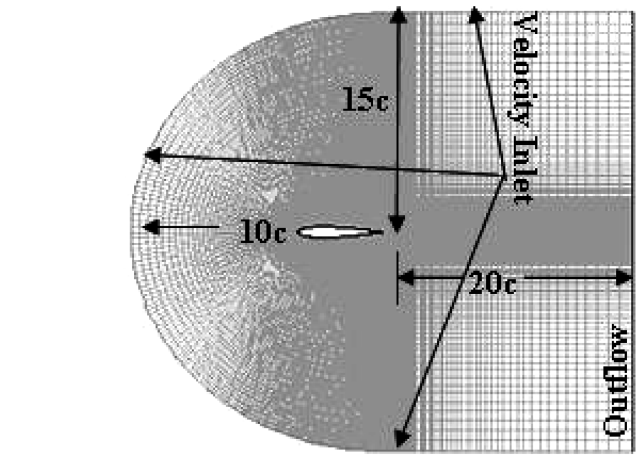

a)

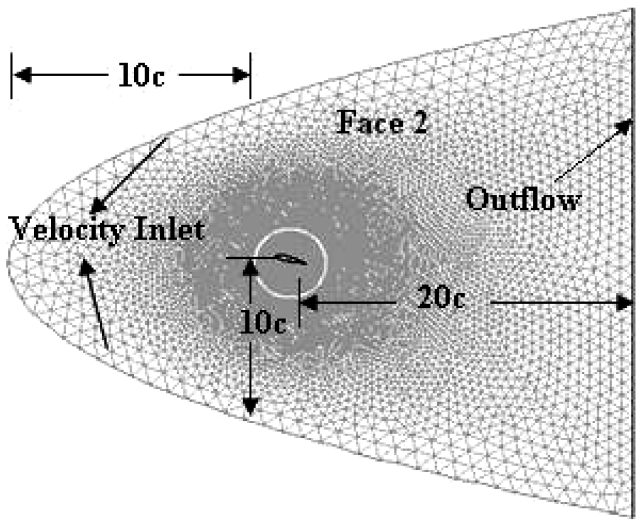

b)

Fig. 1 Computational mesh for the NACA 0015 airfoil: a) stationary configuration, b) pitching configuration.

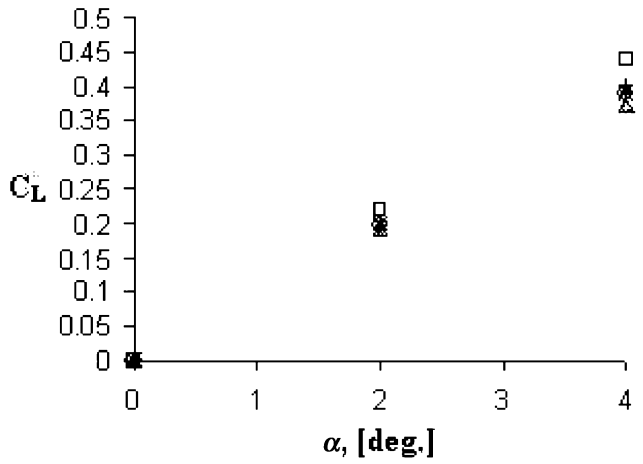

a)

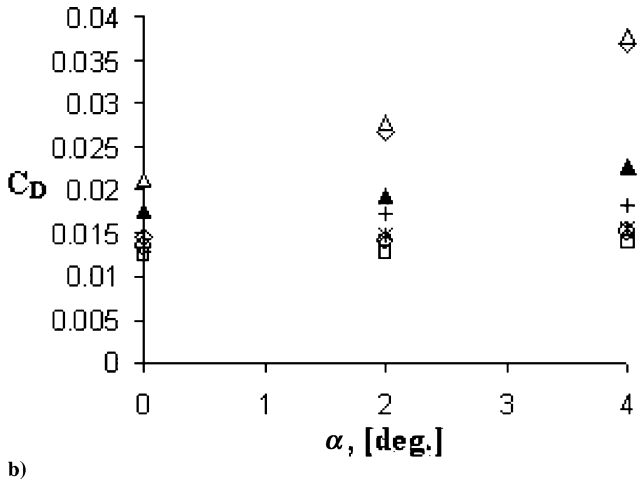

b)

Fig. 2 Comparison of the computational performance of turbulence models with experimental data; ○ is k–ω SST, ▲ is k–ε RNG, ⋄ is Spalart–Almaras (SA), + is k–ε realizable, △ is k–ε standard, * is k–ω standard, □ is experiment [23] (stationary airfoil without the synthetic jet).

flow velocity and pressure are not known before the solution of the problem. No input is required from the user for this boundary condition as Fluent extrapolates the required information from the interior of the domain. As long as the flow at the exit was expected to be well developed and incompressible, the selection of outflow boundary condition at the exit boundary was a reasonable choice. The surface of the airfoil was modeled as a wall. In viscous flows (such as in the present study), the nonslip, or zero tangential velocity boundary condition, was enforced when the wall boundary condition was imposed; the shear stress and associated friction drag were computed based on the flow details in the local flow field.

The mechanics of the synthetic jet resemble those associated with the outward and inward flows observed when one moves a piston forward and backward in a cylinder having a single orifice. In general, air moves out of the cylinder when the piston is moved forward, displacing the volume of air ahead of it. When the piston is moved backward, air is drawn into the cylinder by virtue of the low level suction pressures created in the cylinder cavity. If the displaced volumes associated with the motion of the piston are equal, then the net mass transfer across the port, for all practical purposes, is equal to zero. A synthetic jet functions in a very similar way; periodic flow is coming out of and into the cavity forming a series of successive vortex rings or a "vortex ring train." Ambient fluid is entrained to the vortex ring train resulting in a jetlike flow. Figure 3 shows a schematic of a typical synthetic jet actuator. The velocity boundary in the orifice was described in terms of the following sinusoidal function:

$$A(t) = A_o \sin(\omega_j t) \tag{1}$$

where $A(t)$ is the oscillating nondimensional velocity of the synthetic jet at the orifice during a blowing-suction cycle. Equation (1) was incorporated within the simulation using the user defined function (UDF) in Fluent and C programming language.

Amir and Kontis [24] have developed piezoelectric synthetic jet actuator devices at the University of Manchester, Experimental Aerodynamics & Measurement Technology Laboratory with a typical maximum nondimensional forcing amplitude of 0.75 at nondimensional forcing frequency of 18.67. The authors employed the same frequency and amplitude values for both aerofoil cases examined in the present study. In the pitching airfoil case, a nondimensional forcing frequency of 31.13 and a nondimensional amplitude of 1.88 were also investigated.

The aerofoil was subjected to a harmonic oscillation about its quarter chord axis which was described in terms of the incidence variation, $\alpha(t)$, using the following relation:

$$\alpha(t) = 15 + 10 \sin(\kappa t) \tag{2}$$

The unsteady motion is usually characterized by the similarity parameter κ, known as reduced frequency of the oscillation [25,26]. For the present study, the value of κ was taken as equal to 0.15.

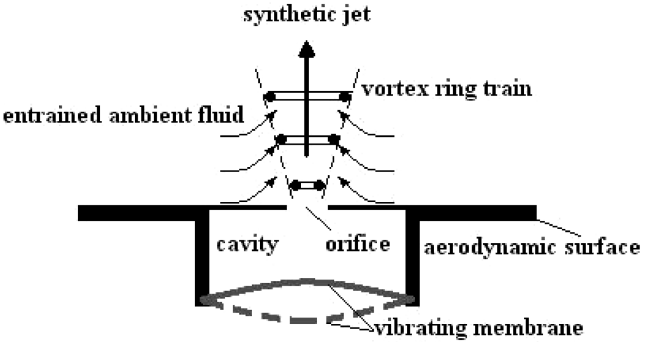

Fig. 3 Schematic of a synthetic jet actuator.

Dynamic Mesh Model

Three-mesh motion strategies were available to accommodate the volume deformation associated with configuration motion: spring smoothing, local remeshing, and dynamic layering. The authors selected the local remeshing method. This choice was made because of three reasons: 1) the remeshing method avoids negative cell volumes when the boundary displacement is very large; 2) the spring-based smoothing method is suitable when the motion is predominantly normal to the boundary zone; and 3) dynamic layering is only suitable when the moving zones are more than one.

Steady State and Unsteady Solution

Although on a microscopic scale, separation point, skin friction, pressure, and drag vary with respect to time, their net values and net effects can be usually considered and modeled accurately as steady properties. Therefore, the baseline simulations for the stationary airfoil case were approximated as steady state, whereas the simulations related to the synthetic jet and the pitching airfoil case were performed as unsteady to capture the time-dependant effects of these flows.

Results and Discussions

Flow over Stationary Airfoil with and Without Synthetic Jet

To calculate the flow parameters such as C_L, C_D, and pressure distributions for the stationary baseline configuration without the

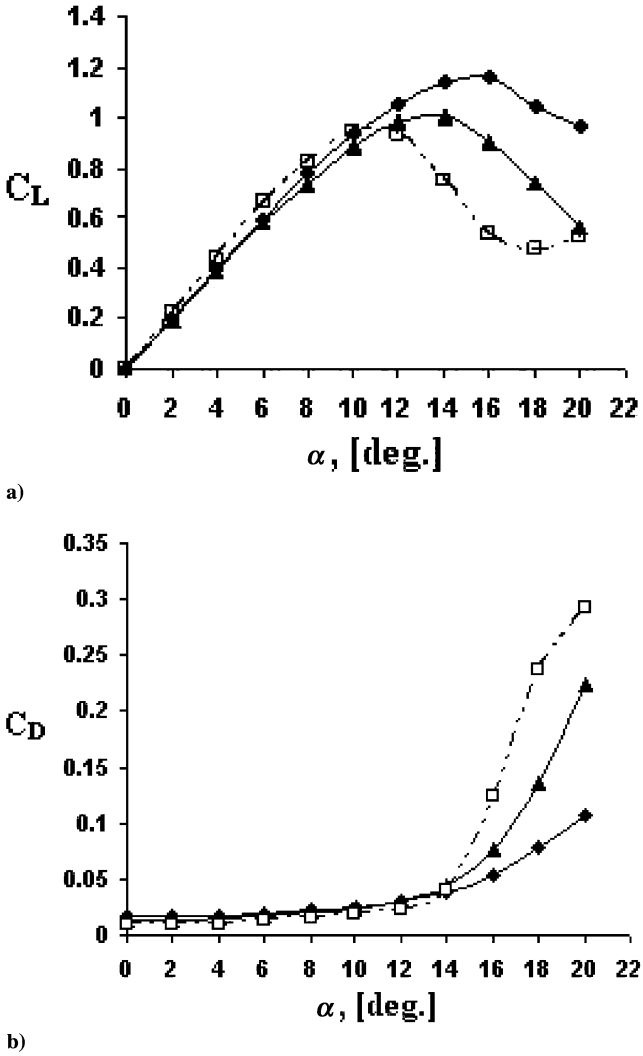

Fig. 4 Comparisons of computational predictions with experimental data; ◆ is k–ε realizable, ▲ is k–ω SST, □ is experiment [23] (stationary airfoil without the synthetic jet).

Table 1 Average percentage of error in the computational and experimental comparisons (stationary airfoil without synthetic jet)

	C_L		C_D	
Turbulence model	Prestall	Poststall	Prestall	Poststall
k–ω SST	2%	30%	0.5%	27%
k–ε realizable	1.5%	72%	0.5%	62%

Table 2 Comparison of the computed mean C_L and C_D at different synthetic jet locations with the results for the no synthetic jet case at 15 deg incidence (stationary airfoil)

L_j, %	C_L (no synthetic jet, k–ω SST)	Mean C_L (with synthetic jet)	C_D (no synthetic jet, k–ω SST)	Mean C_D (with synthetic jet)
36	0.98	1.02	0.03	0.04
32	0.98	1.08	0.03	0.05
28	0.98	1.12	0.03	0.06

synthetic jet, numerical simulations were conducted on a NACA 0015 airfoil at angles of attack ranging from 0 to 20 deg and a Reynolds number of 360,000 based on the chord length of 0.332 m and a freestream velocity of 16 m/s. As it was discussed in section "Turbulence Model Selection Studies," the k–ε realizable and k–ω SST turbulence models were selected for the present simulation. The computed results are presented in Fig. 4. The k–ω SST model predicts the static stall angle at 15 deg whereas the k–ε realizable model predicts it at 17 deg. The experimental value of stall angle is 12 deg. The predictions based on both models are in close agreement with the experimental data [23] in the prestall region. In the poststall region, both models overpredict the experimental lift coefficients and underpredict the experimental drag coefficients. Table 1 provides the average percentage of error in the comparisons of the computational predictions with experiment. Based on the preceding discussion, the k–ω SST model was selected for the remaining simulations over the stationary airfoil with the synthetic jet and the pitching airfoil configurations.

After calculating the flow parameters for the baseline configuration without synthetic jet (stationary airfoil) (BC) case, the synthetic jet was placed at three different chordwise positions to determine its optimum location. The airfoil was at its computed static stall angle (15 deg) and its separation point was located at approximately 40% of the chord length. Initially, the synthetic jet was placed just before the separation point, i.e., 36% of the chord length and then moved away from the separation point at 32% and 28% of the chord length towards the leading edge. Table 2 compares the computed mean lift and drag coefficients at different synthetic jet locations with the results for the no synthetic jet case at 15 deg incidence. These results suggest two interesting findings: 1) lift is increased if the synthetic jet is placed far away from separation point, and 2) drag is reduced if the synthetic jet is placed close to separation point. To support these findings, the pressure coefficient distributions, Fig. 5, were examined. It is evident that the pressure recovery at the trailing edge is larger when the jet is located at 28% of the chord length as compared with the other two locations, i.e., 36 and 32%, implying that the flow is more stable and attached.

To obtain a better understanding of how the synthetic jet might affect the flow over the airfoil, the flow pattern close to the trailing edge was examined; see Fig. 6. The synthetic jet at 28% of the chord length suppressed the separated flow more effectively as compared with the other computed locations.

Based on the computed results and the numerical flow visualization study, imparting movement to flow far away from separation point is suitable if the control goal is to increase lift, whereas the location of the synthetic jet close to separation point is suitable for drag reduction.

Effect of Synthetic Jet at Pre- and Poststall Conditions

The synthetic jet was introduced at 28% of the chord length and the flow field was simulated for angles of attack of 0, 4, 8, 12, 15, 16, and 17 deg. The computed C_L and C_D (obtained from the converged unsteady solution) along with experimental data [23] and the BC case results are presented in Fig. 7.

The computed results show that: 1) increase in lift from 0.98 at 14 deg angle of attack (BC case) to 1.24 at 17 deg angle of attack [synthetic jet configuration (SJC) case] is achieved at the cost of increase in drag, and 2) the lift increment due to the synthetic jet is more pronounced at poststall conditions, i.e., 15, 16, and 17 deg as compared with prestall conditions. This observation contradicts previous findings by other researchers [27–29] where C_L enhancement was more pronounced in the prestall conditions. The difference in the results could be due to the difference in the location of the synthetic jet relative to the separation point. As the separation point moves towards the leading edge with increasing incidence, its distance from the synthetic jet will decrease and therefore the control

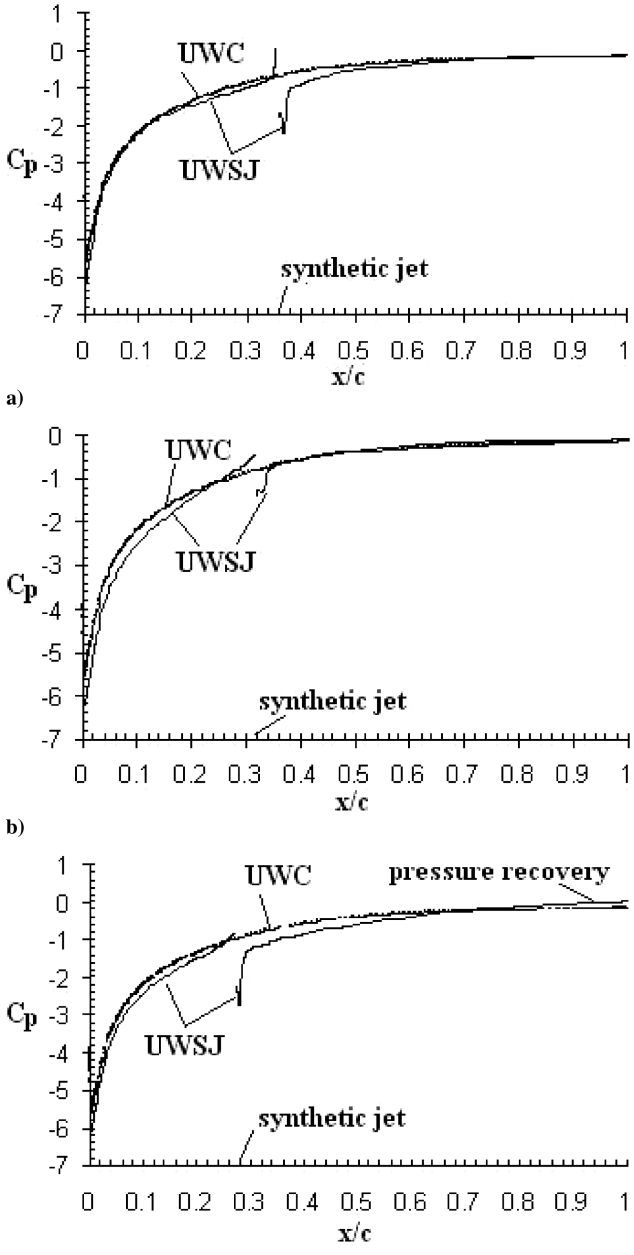

Fig. 5 Pressure coefficient distributions along the leeward side without synthetic jet (UWC) and with synthetic jet (UWSJ) at 15 deg incidence: a) $L_j = 36\%$, b) $L_j = 32\%$, and c) $L_j = 28\%$ (stationary airfoil).

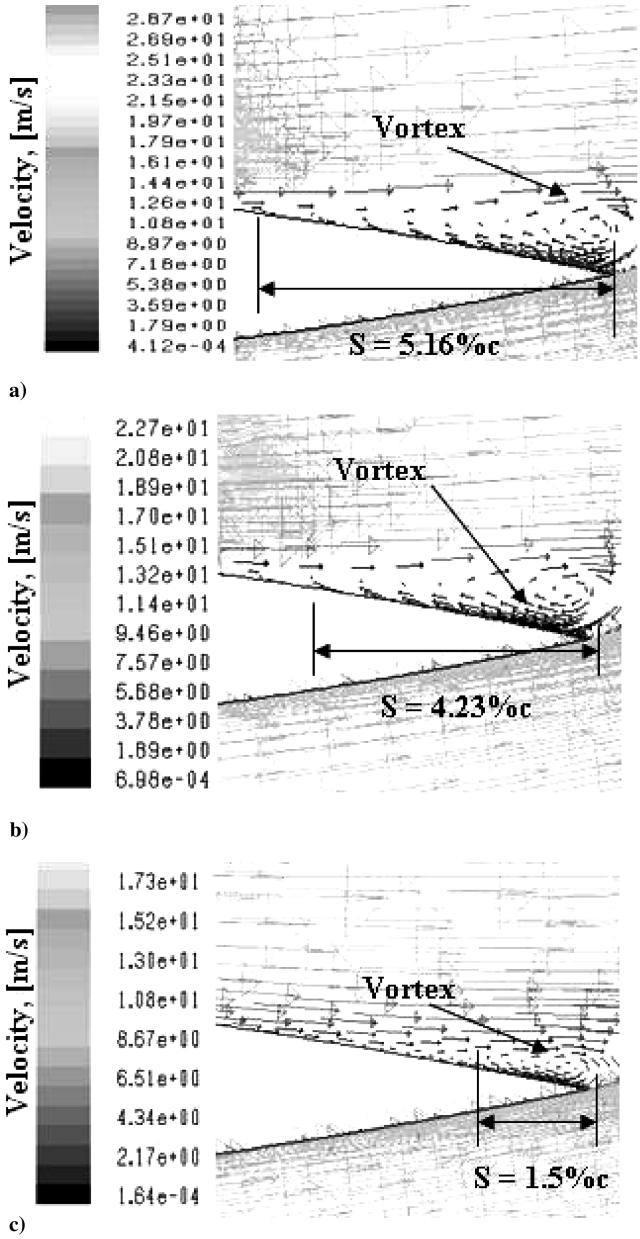

Fig. 6 Flow pattern and velocity vectors at the trailing edge region: a) $L_j = 36\%$, b) $L_j = 32\%$, and c) $L_j = 28\%$ (15 deg incidence, stationary airfoil, S = separation length).

effectiveness of the synthetic jet will change. Thus, fixing the location of the synthetic jet over an entire incidence range is not an effective design solution.

Pressure Distributions with Synthetic Jet Located at 28% of the Chord Length

The pressure distributions were studied for 0, 4, 8, 12, 15, 16, and 17 deg angles of attack. The results indicate that the pressure recovery after the synthetic jet on the suction side of the airfoil is larger at incidences over 12 deg; see Fig. 8. This means that the pressure coefficient increases downstream of the synthetic jet on the suction side, indicating reduced separation region.

Flow over Pitching Airfoil Without Synthetic Jet

The NACA 0015 airfoil was allowed to oscillate in pitch about its quarter chord with amplitude of 10 deg about a 15 deg mean angle of attack, which is the computed stall angle for the stationary airfoil, at a Reynolds number of 360,000 based on the chord length of 0.332 m and a freestream velocity of 16 m/s.

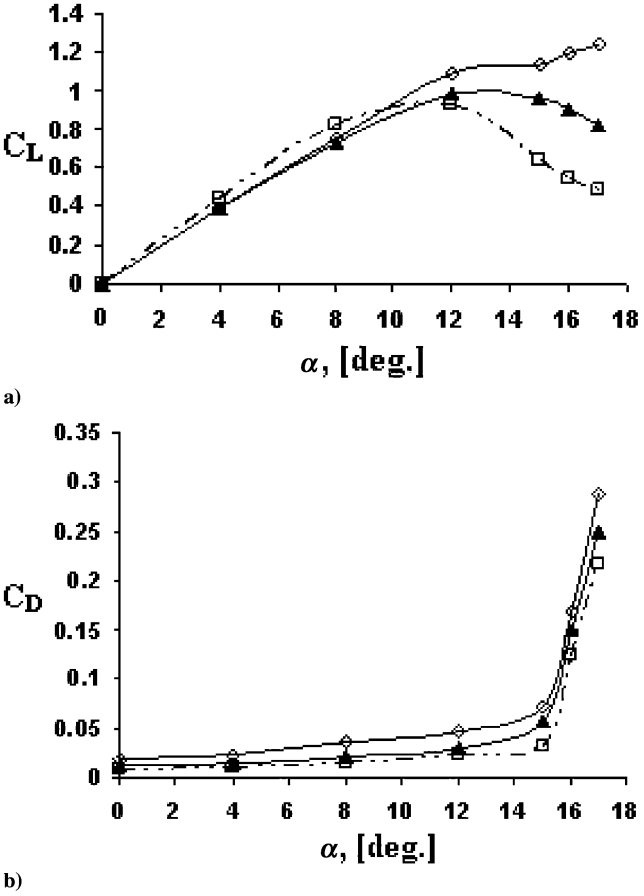

Fig. 7 Effect of synthetic jet on a) C_L variation with α, and b) C_D variation with α; ⋄ is k–ω SST (SJC case), ▲ is k–ω SST (BC case), □ is experiment (without synthetic jet) [23] (stationary airfoil).

Figure 9 shows the flow development around the airfoil pitching between 5 and 25 deg with a reduced frequency of 0.15. In Fig. 9a, the flow is attached to both sides of the airfoil until 12 deg incidence. Then a vortex starts to form at the trailing edge (TE); see Fig. 9b. With increasing incidence, the trailing vortex (clockwise in rotation) grows in size; see Figs. 9c and 9d. In addition, a small leading edge (LE) vortex forms approximately at 15 deg incidence. The leading edge vortex is also clockwise in its rotation. The trailing edge vortex grows in size as the airfoil continues to pitch up until 20 deg incidence and then another trailing edge vortex is formed (anticlockwise in its rotation); see Fig. 9e. It is observed that all three vortices grow in size as the airfoil continues its pitch-up cycle. The growth of the leading vortex is slow as compared with the trailing edge vortices and remains attached to the surface of the airfoil; see Figs. 9f–9h. Finally, the trailing edge vortex sheds from the airfoil surface at approximately 24.7 deg incidence; see Fig. 9i. With the shedding of the trailing edge vortex, the other two vortices reduce in size; see Figs. 9j and 9k. As the airfoil starts its pitch-down cycle, the separation point starts to move towards the trailing edge, indicating reduction in size of the remaining vortices. Finally, flow reattachment is observed close to 10 deg incidence; see Fig. 9n. The observed phenomena repeat themselves during each pitch-up and pitch-down cycle.

Flow over Pitching Airfoil with Synthetic Jet

Effect of Nondimensional Forcing Amplitude of 0.75 and Frequency of 18.67

The synthetic jet with nondimensional forcing frequency and amplitude of 18.67 and 0.75, respectively, was introduced at 28% of the chord length. The computed C_L, C_D, and C_M distributions are presented in Fig. 10. In the same figure, the baseline configuration without synthetic jet (pitching airfoil) (BCPA) case is also compared

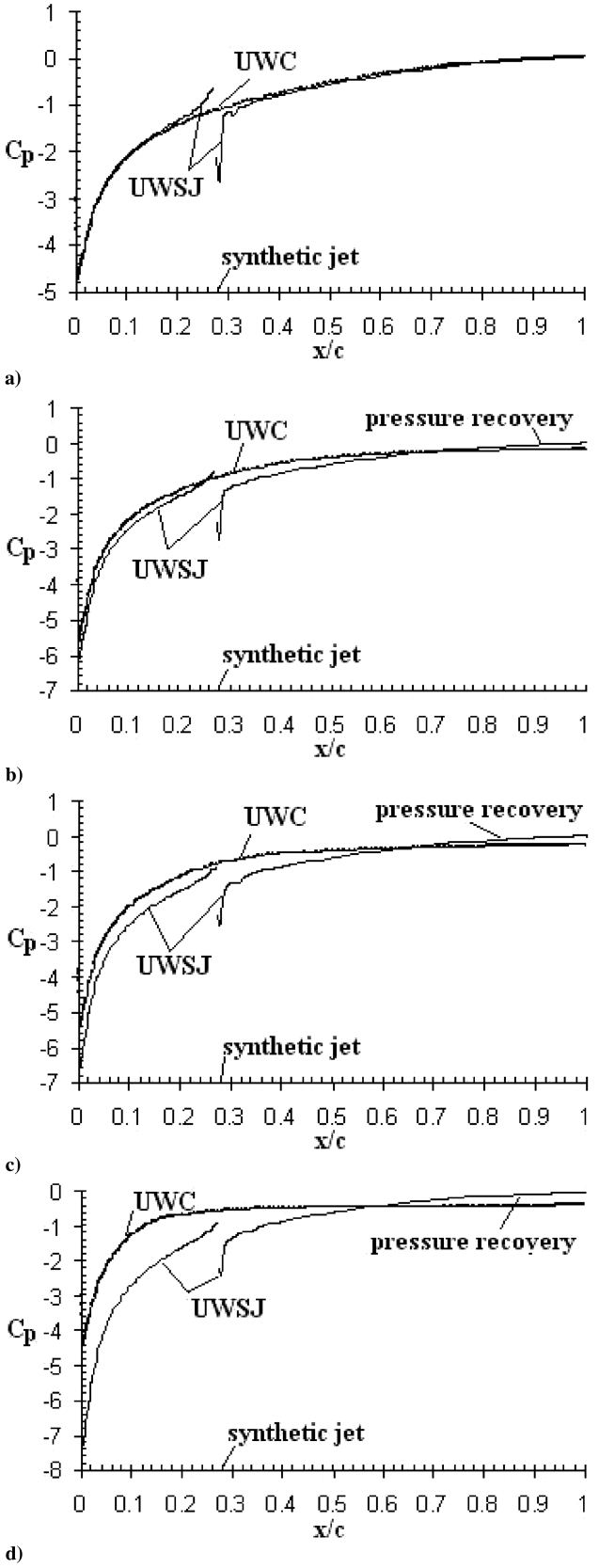

Fig. 8 Pressure coefficient distributions along the leeward side at $L_j = 28\%$: a) $\alpha = 8$ deg, b) $\alpha = 15$ deg, c) $\alpha = 16$ deg, and d) $\alpha = 17$ deg (stationary airfoil).

with experimental data from [26]. Table 3 provides the average percentage of error in the comparisons of the computational predictions for the BCPA case with experiment. In general, computations overpredict the experimental results at all incidences.

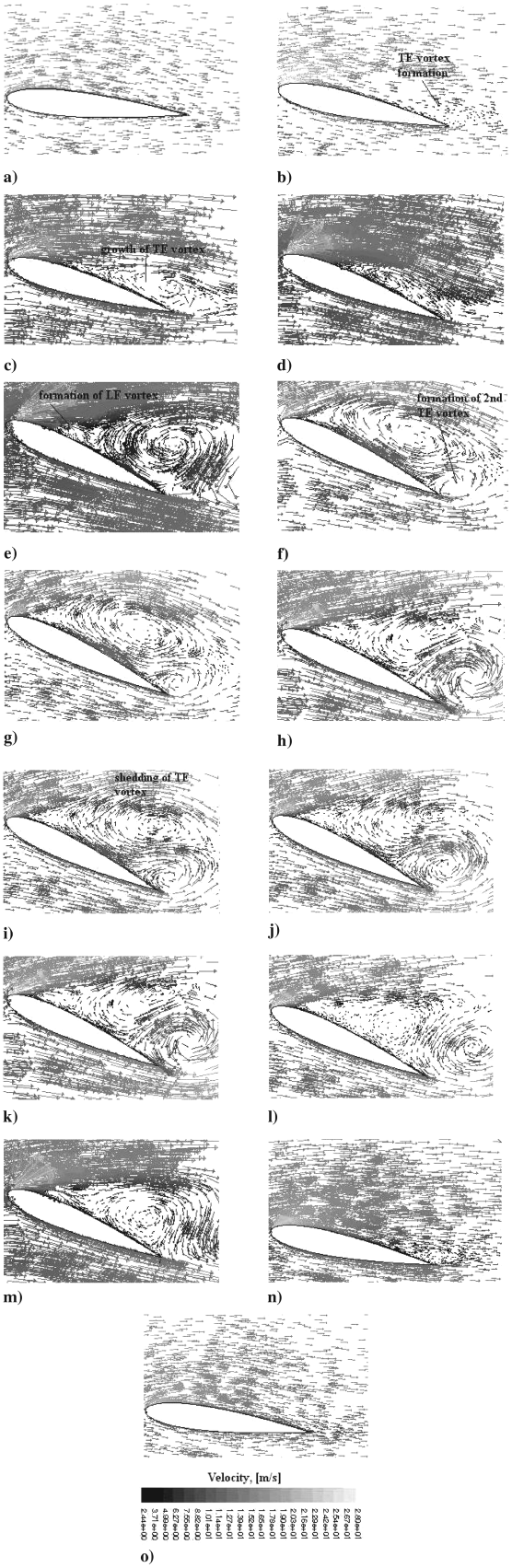

Fig. 9 Flow pattern and velocity vectors for BCPA case: a) pitch-up, $\alpha = 9$ deg; b) pitch-up, $\alpha = 14$ deg; c) pitch-up, $\alpha = 16$ deg; d) pitch-up, $\alpha = 18$ deg; e) pitch-up, $\alpha = 19$ deg; f) pitch-up, $\alpha = 20$ deg; g) pitch-up, $\alpha = 22$ deg; h) pitch-up, $\alpha = 23$ deg; i) pitch-up, $\alpha = 24.6$ deg; j) pitch-down, $\alpha = 24$ deg; k) pitch-down, $\alpha = 23$ deg; l) pitch-down, $\alpha = 22$ deg; m) pitch-down, $\alpha = 20$ deg; n) pitch-down, $\alpha = 15$ deg; o) pitch-down, $\alpha = 10$ deg.

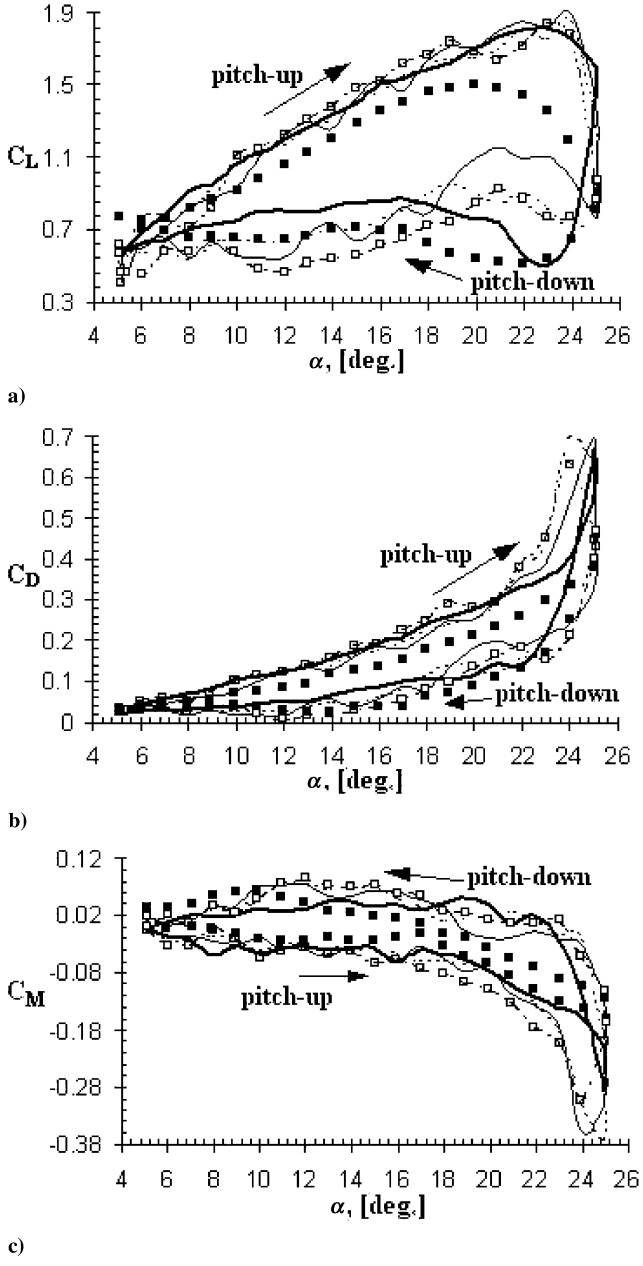

Fig. 10 Effect of synthetic jet on: a) C_L variation with α, b) C_D variation with α, and c) C_M variation with α; solid bold line is BCPA, dashed line is SJCPA with $A_o = 0.75$ and $\omega_j = 18.67$, □ is SJCPA with $A_o = 1.88$ and $\omega_j = 18.67$, solid line is SJCPA with $A_o = 0.75$ and $\omega_j = 33.13$, ■ is experiment (without synthetic jet) [26] (pitching airfoil).

For the BCPA case, the maximum C_L was 1.81 at 22.8 deg. The maximum experimental value of C_L was 1.51 at 20 deg; see Fig. 10a. The introduction of the synthetic jet caused an increase in C_L from 1.81 to 1.85. In addition, the incidence of maximum C_L moved from 22.8 to 23.85 deg. However, this increase in C_L was accompanied by an increase in C_D, as compared with the BCPA case, from 0.67 to 0.69; see Fig. 10b. The maximum experimental value of C_D was 0.38. For the BCPA case, an increase in C_M was predicted throughout the pitch-up cycle and the pitch-down cycle until 24.97 deg; see Fig. 10c. A recovery in C_M was calculated during the pitch-up cycle for the synthetic jet configuration for pitching airfoil (SJCPA) case. The maximum C_M was −0.38 as compared with −0.28 for the BCPA case; see Fig. 10c. The maximum experimental value of C_M was −0.13 at 24 deg. The computed results suggest that the introduction of the synthetic at 28% of the chord length leads to an increase in C_L and a shift in maximum C_L incidence at a cost of an increase in C_D and a more negative C_M.

Table 3 Average percentage of error in the computational and experimental comparisons [23] (pitching airfoil without synthetic jet)

	C_L	C_D	C_M
Pitch-up cycle	20%	35%	17%
Pitch-down cycle	18%	30%	29%

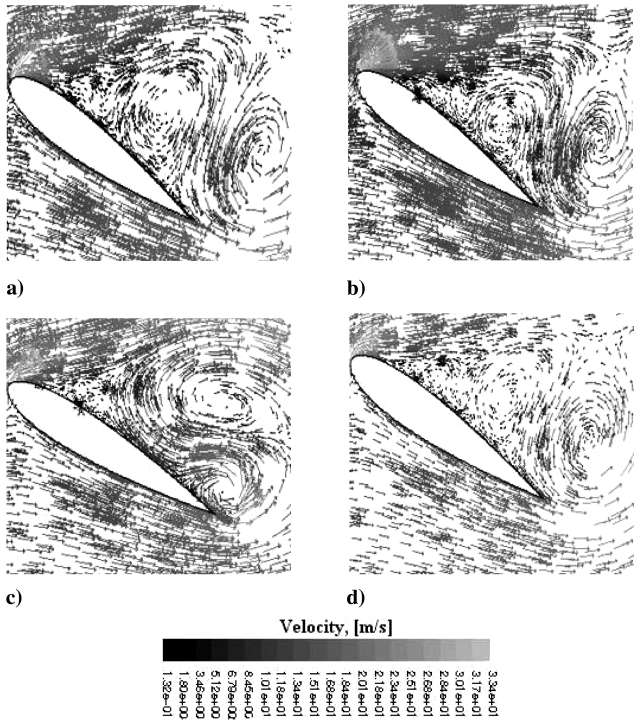

Fig. 11 Comparison of flow pattern and velocity vectors for all pitching cases: a) BCPA, b) SJCPA with $A_o = 0.75$ and $\omega_j = 18.67$, c) SJCPA with $A_o = 1.88$ and $\omega_j = 18.67$, and d) SJCPA with $A_o = 0.75$ and $\omega_j = 33.13$.

Effect of Forcing Amplitude

The forcing amplitude was increased from 0.75 to 1.88 while keeping the forcing frequency fixed at 18.67. The computed C_L, C_D, and C_M distributions are presented in Fig. 10. The maximum C_L was 1.83 as compared with 1.85 and 1.81 for SJCPA with 0.75 forcing amplitude and BCPA, respectively. The maximum lift incidence was 22.97 deg as compared with 23.85 and 22.8 deg for SJCPA with 0.75 forcing amplitude and BCPA, respectively. The maximum C_D was 0.63 as compared with 0.69 and 0.67 for SJCPA with 0.75 forcing amplitude and BCPA, respectively, indicating a reduction of drag with increasing forcing amplitude. The maximum C_M was −0.31 as compared with −0.38 and −0.28 for SJCPA with 0.75 forcing amplitude and BCPA, respectively. In summary, if the design goal was to achieve drag reduction, then a synthetic jet with higher forcing amplitude would be the better choice for a pitching airfoil.

Effect of Forcing Frequency

The forcing frequency was increased from 18.67 to 31.13 while keeping the forcing amplitude fixed at 0.75. The computed C_L, C_D, and C_M distributions are presented in Fig. 10. The maximum C_L was 1.89 as compared with 1.85, 1.83, and 1.81 for SJCPA with 0.75 forcing amplitude and 18.67 forcing frequency, SJCPA with 1.88 forcing amplitude and 18.67 forcing frequency, and BCPA, respectively. The maximum lift incidence was 24.11 deg as compared with 23.85, 22.97, and 22.8 deg for SJCPA with 0.75 and 18.67, SJCPA with 1.88 and 18.67, and BCPA, respectively. The maximum C_D was 0.70 as compared with 0.69, 0.63, and 0.67 for SJCPA with 0.75 and 18.67, SJCPA with 1.88 and 18.67, and BCPA,

respectively. The maximum C_M was −0.36 as compared with −0.38, −0.31, and −0.28 for SJCPA with 0.75 and 18.67, SJCPA with 1.88 and 18.67, and BCPA, respectively. In summary, if the design goal was to achieve lift enhancement, then a synthetic jet with higher forcing frequency would be the better choice for a pitching airfoil.

Numerical Flow Visualization

Figure 11 compares the flow patterns for all pitching cases at incidence 22 deg. The general sequence of events is identical to that observed for the BCPA case (see Fig. 9); however, the specific flow events occur at different incidences and time steps (see Fig. 11 and [30]). This implies that the synthetic jet affects the sequence and timing of vortex formation and shedding for each case. However, even with increased forcing frequency or amplitude, it is not able to suppress the vortex shedding process. It is conjectured that the increase in airfoil performance with the introduction of the synthetic jet is due to the formation and shedding of the trailing edge vortex occurring at different incidences for each case. Experimental studies are underway at the University of Manchester, Experimental Aerodynamics & Measurement Technology Laboratory to verify the accuracy of the computational predictions especially for the pitching airfoil with a synthetic jet configuration.

Conclusions

A series of numerical simulations were conducted to investigate the control effectiveness of a synthetic jet on the aerodynamic performance and characteristics of a stationary and a pitching NACA 0015 aerofoil.

For a stationary airfoil, the increase in lift due to the synthetic jet was more pronounced at high incidences (10–20 deg). The effectiveness of the synthetic jet was reduced at low incidences (4–10 deg). At all incidences, the increase in lift was accompanied by an increase in drag. Imparting movement of flow far away from separation point is useful if lift enhancement is required while the location of synthetic jet close to separation point is suitable for drag reduction. The pressure recovery at the trailing edge was larger when the synthetic jet was located at 28% of the chord length. The pressure recovery on the suction side of the airfoil after the synthetic jet was larger at incidences over 12 deg. The k–ω SST model successfully predicted the flow events.

For a pitching airfoil, a single synthetic jet was not able to suppress the vortex formation and shedding; however, the overall airfoil performance was enhanced. A synthetic jet operating at higher forcing amplitudes is suitable for drag reduction, whereas a synthetic jet operating at higher forcing frequencies is suitable for lift enhancement. The k–ω SST successfully captured the sequence of flow events such as development of the vortex at the trailing edge, streamwise movement of the vortex, and shedding of the vortex downstream.

References

[1] Talay, T. A., "Introduction to the Aerodynamics of Flight," NASA Langley SP-367, pp. 68–69, 1975.

[2] Smith, H. C., *The Illustrated Guide to Aerodynamics*, 2nd ed., Tab, New York, 1992, pp. 46–47.

[3] Gad-el-Hak, M., "Control of Low-Speed Airfoil Aerodynamics," *AIAA Journal*, Vol. 28, No. 9, 1990, pp. 1537–1552.

[4] McCroskey, L., "Dynamic Stall on Advanced Airfoil Sections," *Journal of the American Helicopter Society*, Vol. 26, No. 3, July 1981, pp. 40–50.

[5] McCroskey, W. J., "The Phenomenon of Dynamic Stall," NASA TM-81264, 1981.

[6] Gault, D. E., "A Correlation of Low-Speed, Airfoil-Section Stalling Characteristics with Reynolds Number and Airfoil Geometry," NACA TN-3963, 1957.

[7] Geissler, W., Trenker, M., and Sobieczky, H., "Active Dynamic Flow Control Studies on Rotor Blades," *Deutsches Zentrum für Luft- und Raumfahrt e.V.*, Institut für Trömungsmechanik, Göttingen, Germany, D-37073, 1992.

[8] Geissler, W., and Sobieczky, H., "Unsteady Flow Control on Rotor Airfoil," AIAA Paper 95-0234, 1995.

[9] Prouty, R. W., *Helicopter Performance, Stability, and Control*, PWS Engineering, New York, 1986.

[10] Bursnall, W. J., "Experimental Investigation of the Effects of Vortex Generators on the Maximum Lift of a 6-Percent-Thick Symmetrical Circular-Arc Airfoil Section," NACA RM-L52G24, 1952.

[11] Zhou, M. D., Fernholz, H. H., Ma, H. Y., Wu, J. Z., and Wu, J. M., "Vortex Capture by a Two-Dimensional Airfoil with a Small Oscillating Leading-Edge Flap," AIAA Paper 93-3266, 1993.

[12] McAlister, K. W., and Tung, C., "Suppression of Dynamic Stall with a Leading-Edge Slat on a VR-7 Airfoil," NASA TP-3357, 1993.

[13] Lee, S., McAlister, K. W., and Tung, C., "Characteristics of a Deformable Leading Edge for High Performance Helicopter Rotor," AIAA Paper 93-3526, 1993.

[14] Carr, L. W., Chandrasekhara, M. S., Wilder, M. C., and Noonan, K. W., "Effect of Compressibility on Suppression of Dynamic Stall Using a Slotted Airfoil," *Journal of Aircraft*, Vol. 38, No. 2, 2001, pp. 296–309.

[15] Shih, C., Beahn, J., Krothapalli, A., and Chandrasekhara, M. S., "Control of Compressible Dynamic Stall Using Microjets," *Proceedings of the 2003 ASME Fluids Engineering Summer Meeting*, American Society of Mechanical Engineers, 2003, pp. 204–212.

[16] Greenblatt, D., and Wygnanski, I., "Dynamic Stall Control by Oscillatory Forcing," AIAA Paper 98-0676, 1998.

[17] Post, M., "Plasma Actuators for Separation Control on Stationary and Oscillating Airfoils", Ph.D. Dissertation, Univ. of Notre Dame, South Bend, IN, April 2004.

[18] Chen, F., and Beeler, G., "Virtual Shaping of a Two-Dimensional NACA 0015 Airfoil Using Synthetic Jet Actuator," AIAA Paper 2002-3273, 2002.

[19] Smith, B. L., and Glezer, A., "Jet Vectoring Using Synthetic Jets," *Journal of Fluid Mechanics*, Vol. 458, May 2002, pp. 1–34.

[20] Leonard, B. P., "A Stable and Accurate Convective Modeling Procedure Based on Quadratic Upstream Interpolation," *Computer Methods in Applied Mechanics and Engineering*, Vol. 19, No. 1, June 1979, pp. 59–98.

[21] Patankar, S. V., and Spalding, D. B., "A Calculation Procedure for Heat, Mass and Momentum Transfer in Three-Dimensional Parabolic Flow", *International Journal of Heat and Mass Transfer*, Vol. 15, No. 10, Oct. 1972, pp. 1787–1806.

[22] *Fluent 6.1 User's Guide*, Fluent, Ltd., Sheffield, U.K. Dec. 2003.

[23] Sheldahl, R. E., and Klimas, P. C., "Aerodynamic Characteristics of Seven Airfoil Sections Through 180 Degrees Angle of Attack," Sandia National Laboratories, Albuquerque, NM, http://www.cyberiad.net/library/airfoils/foildata/n0015cl/cd.htm [cited May 2004].

[24] Amir, M., and Kontis, K., "Design and Applications of a PZT Synthetic Jet Actuator", AIAA Paper 05-0345, 2005.

[25] Barakos, G., Drikakis D., and Leschziner, M., "Numerical Investigation of Dynamic Stall Phenomenon Using Non-Linear Eddy-Viscosity Model," AIAA Paper 98-2740, 1998.

[26] Sun, M., and Sheikh, S. R., "Dynamic Stall Suppression on an Oscillating Airfoil by Steady and Unsteady Tangential Blowing," *Aerospace Science and Technology*, Vol. 3, No. 6, Sept. 1999, pp. 355–366.

[27] Hsiao, F. B., Liang, P. F., and Huang, C. Y., "High-Incidence Airfoil Aerodynamics Improvement by Leading-Edge Oscillating Flap," *Journal of Aircraft*, Vol. 35, No. 3, pp. 508–510, 1998.

[28] Ekaterinaris, J. A., "Prediction of Active Flow Control Performance on Airfoils and Wings," *Aerospace Science and Technology*, Vol. 8, No. 5, July 2004, pp. 401–410.

[29] Hassan, A. A., and JanakiRam, R. D., "Effects of Zero-Mass Synthetic Jets on the Aerodynamics of the NACA 0012 Airfoil," AIAA Paper 97-2326, 1997.

[30] Rehman, A., "Computational Studies on the Control Effectiveness of Synthetic Jets for Aerodynamics Applications," M.Phil. Dissertation, UMIST, Manchester, England, Dec. 2004.